

Variable-Agnostic Causal Exploration for Reinforcement Learning

Minh Hoang Nguyen¹(✉), Hung Le¹, Svetha Venkatesh¹
¹Applied Artificial Intelligence Institute (A2I2),
 Deakin University, Australia
 {s223669184, thai.le, svetha.venkatesh}@deakin.edu.au

July 18, 2024

Abstract

Modern reinforcement learning (RL) struggles to capture real-world cause-and-effect dynamics, leading to inefficient exploration due to extensive trial-and-error actions. While recent efforts to improve agent exploration have leveraged causal discovery, they often make unrealistic assumptions of causal variables in the environments. In this paper, we introduce a novel framework, Variable-Agnostic Causal Exploration for Reinforcement Learning (VAC-ERL), incorporating causal relationships to drive exploration in RL without specifying environmental causal variables. Our approach automatically identifies crucial observation-action steps associated with key variables using attention mechanisms. Subsequently, it constructs the causal graph connecting these steps, which guides the agent towards observation-action pairs with greater causal influence on task completion. This can be leveraged to generate intrinsic rewards or establish a hierarchy of subgoals to enhance exploration efficiency. Experimental results showcase a significant improvement in agent performance in grid-world, 2d games and robotic domains, particularly in scenarios with sparse rewards and noisy actions, such as the notorious Noisy-TV environments.

Keywords: Reinforcement Learning, Causality, Deep RL.

1 Introduction

Reinforcement learning (RL) is a machine learning paradigm wherein agents learn to improve decision-making over time through trial and error [25]. While RL has demonstrated remarkable success in environments with dense rewards [15, 23], it tends to fail in case of sparse rewards where the agents do not receive feedback for extended periods, resulting in unsuccessful learning. Such scarcity of rewards is common in real-world problems: e.g., in a search mission, the reward is only granted upon locating the target. Prior studies tackle this problem by incentivizing exploration through intrinsic rewards [26, 3], motivating exploration of the unfamiliar, or with hierarchical reinforcement learning (HRL) [13, 31, 17]. However, these methods encounter difficulties when scaling up to environments with complex structures as they neglect the causal dynamics of the environments. Consider the example of a search in two rooms (Fig. 1(a, b)), where the target is in the second room, accessible only by opening a “door” with a “key” in the first room. Traditional exploration methods might force the agent to explore all corners of the first room, even though only the “key” and “door” areas are crucial. Knowing that the action "pick up key" is the cause

of the effect "door opened" will prevent the agent from aimlessly wandering around the door before the key is acquired. Another challenge with these approaches is the Noisy-TV problem [3], where the agent excessively explores unfamiliar states and actions that may not contribute to the ultimate task. These inefficiencies raise a new question: *Can agents effectively capture causality to efficiently explore environments with sparse rewards and distracting actions?*

Inspired by human reasoning, where understanding the relationship between the environmental variables (EVs) helps exploration, causal reinforcement learning (CRL) is grounded in causal inference [29]. CRL research often involves two phases: (i) causal structure discovery and (ii) integrating causal knowledge with policy training [29]. Recent studies have demonstrated that such knowledge significantly improves the sample efficiency of agent training [8, 22, 30]. However, *current approaches often assume access to all environmental causal variables and pre-factorized environments* [22, 8], simplifying the causal discovery phase. In reality, causal variables are not given from observations, and constructing a causal graph for all observations becomes a non-trivial task due to the computational expense associated with measuring causality. Identifying EVs crucial for downstream tasks becomes a challenging task, thereby limiting the effectiveness of CRL methods. These necessitate the identification of a subset of crucial EVs before discovering causality.

This paper introduces the ***Variable-Agnostic Causal Exploration for Reinforcement Learning (VACERL)*** framework to address these limitations. The framework is an iterative process consisting of three phases: "*Crucial Step Detection*", "*Causal Structure Discovery*", and "*Agent Training with Causal Information*". The first phase aims to discover a set of crucial observation-action steps, denoted as the $SCOAS$. The term "crucial observation-action step" refers to an observation and an action pair stored in the agent's memory identified as crucial for constructing the causal graph. We extend the idea of detecting crucial EVs to detecting crucial observation-action steps, motivated by two reasons. Firstly, variables in the environment are associated with the observations, e.g., the variable "key" corresponds to the agent's observation of the "key". Secondly, actions also contribute to causality, e.g., the agent cannot use the "key" without picking it up. One way of determining crucial observation-action steps involves providing the agent with a mechanism to evaluate them based on their contribution to a meaningful task [9]. We implement this mechanism using a Transformer architecture, whose task is to predict the observation-action step leading to the goal given past steps. We rank the significance of observation-action steps based on their attention scores [28] and pick out the top-ranking candidates since the Transformer must attend to important steps to predict correctly.

In Phase 2, we adapt causal structure learning [10] to discover the causal relationships among the observation-action steps identified in the discovered $SCOAS$ set, forming a causal graph G . The steps serve as the nodes of the causal graph, while the edges can be identified through a two-phase iterative optimization of the functional and structural parameters, representing the Structure Causal Model (SCM). In Phase 3, we train the RL agent based on the causal graph G . To prove the versatility of our approach in improving the sample efficiency of RL agents, we propose two methods to utilize the causal graph: (i) formulate intrinsic reward-shaping equations grounded on the captured causal relationship; (ii) treat the nodes in the causal graph as subgoals for HRL. During subsequent training, the updated agent interact with the environments, collecting new trajectories for the agent memory used in the next iteration of Phase 1.

In our experiments, we use causally structured grid-world and robotic environments to empirically evaluate the performance improvement of RL agents when employing the two approaches in Phase 3. This improvement extends not only to scenarios with sparse rewards but also to those

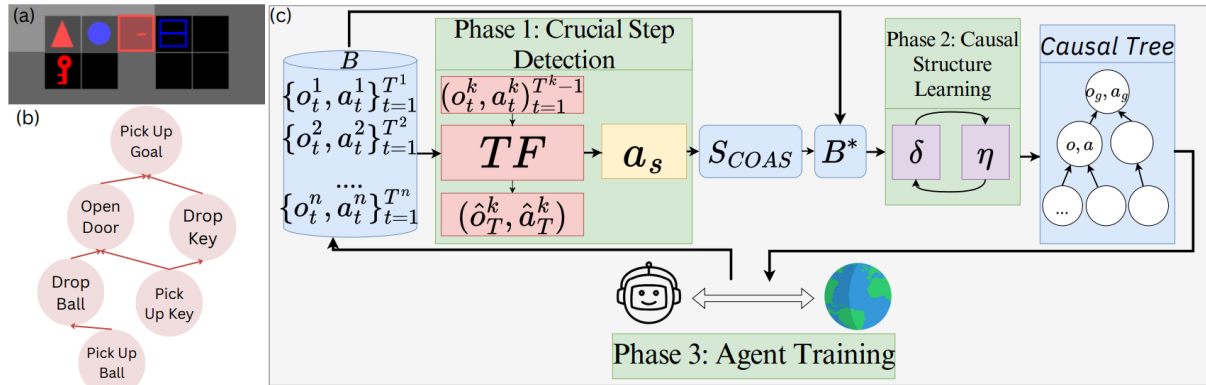


Figure 1: **(a)**: A causally structured environment (MG-2): the agent, starting in the left room is given a +1 reward when it picks up the blue box located in the right room. **(b)**: A possible causal the graph represents the ideal causality steps for the environment in (a): pick up and then drop the ball in another position; pick up the key to open the door; and ultimately pick up the target goal. **(c)**: VACERL framework. During the process of the agent training (initially, a random policy is used) in the environment, we extracted any successful trajectories and filled buffer B . The Transformer (TF) model, trained using B , takes input $\{o_t^k, a_t^k\}_{t=1}^{T^k-1}$ to predict $(\hat{o}_T^k, \hat{a}_T^k)$. TF 's attention score (a_s) is used to determine the set $SCOAS$ and buffer B^* . Parameters δ and η of the SCM are optimized using B^* . We extract a causal hierarchy tree from the causal graph and use it to design the approaches employed for agent training.

influenced by the Noisy-TV problem. We also investigate the contributions of the core components of VACERL, analyzing the emerging learning behaviour that illustrates the captured causality of the agents. Our main contributions can be summarized as:

- We present a novel **VACERL** framework, which autonomously uncovers causal relationships in RL environments without assuming environmental variables or factorized environments.
- We propose two methods to integrate our framework into common RL algorithms using intrinsic reward and hierarchical RL, enhancing exploration efficiency and explaining agent behaviour.
- We create causally structured environments, with and without Noisy-TV, to evaluate RL agents' exploration capabilities, demonstrating the effectiveness of our approach through extensive experiments.

2 Related Work

Causal Reinforcement Learning (CRL) is an emerging field that integrates causality and reinforcement learning (RL) to enhance decision-making in RL agents, addressing limitations associated with traditional RL, such as sample efficiency and explainability [29]. CRL methods can be categorized based on their experimental setups, whether they are online or offline [29]. Online-CRL involves real-time interaction with the environment [5, 8, 30, 22], while Offline-CRL relies on learning from a fixed previously collected dataset [24, 18]. Our framework operates

online, using trajectories from an online policy for an agent training while simultaneously constructing the underlying causal graph. Prior works in CRL have focused on integrating causal knowledge into RL algorithms and building causal graphs within the environment. Pitis et al., [18] use Transformer model attention weights to generate counterfactual data for training RL agents, while Coroll et al., [5] use causal effect measurement to build a hierarchy of controllable effects. Zhang et al., [32] measure the causal relationship between states and actions with the rewards and redistribute the rewards accordingly. For exploration purposes, CRL research integrates causal knowledge by rewarding the agents when they visit states with higher causal influence [22, 30] or treating the nodes of the causal graph as potential subgoals in HRL [8]. Zhang et al., [30] measure the average causal effect between a predefined group of variables and use this as a reward signal, meanwhile, Seitzer et al., [22] propose conditional mutual information as a measurement of causal influence and use it to enhance the exploration of the RL agent. Hu et al., [8] introduce a continuous optimization framework, building a causal structure through a causality-guided intervention and using it to define hierarchical subgoals. Despite advancements, previous methods often assume prior knowledge of EVs and the ability to factorize the environment accordingly. Our framework autonomously detects crucial steps associated with the key EVs, enabling causal structure learning without predefined EVs, thus, distinguishing it from previous methods. The causal graph uncovered by VACERL is versatile and can complement existing RL exploration methods, such as intrinsic reward motivation or as hierarchical subgoals.

Intrinsic Reward Motivation addresses inefficient training in sparse reward RL environments; an issue associated with random exploration techniques like ϵ -greedy [2]. The core idea underlying these motivation strategies is to incorporate intrinsic rewards, which entail adding bonuses to the environment rewards to facilitate exploration [2, 26, 3]. These methods add bonuses to environment rewards to encourage exploration, either based on prediction error [3] or count-based criteria [2, 26]. However, they struggle to scale to complex structure environments, especially in the scenario of Noisy-TV, where the agent becomes excessively curious about unpredictable states and ignores the main task [3]. VACERL tackles this by incorporating a mechanism to identify essential steps for the primary task and construct the causal graph around these steps, thus, enabling the agent to ignore actions generating noisy-TV.

Goal-conditioned Hierarchical Reinforcement Learning (HRL) is another approach that is used to guide agent exploration. Levy et al., [13] propose a multilevel policies framework, in which each policy is trained independently and the output of higher-ranking policies are used as subgoals for lower-level policies. Zhang et al., [31] propose an adjacency constraint method to restrict the search space of subgoals, whereas, Pitis et al., [17] introduce a method based on maximum entropy gain motivating the agent to pursue past achieved goals in sparsely explored areas. However, traditional HRL methods often rely on random subgoals exploration, which has shown inefficiency in learning high-quality hierarchical structures compared to causality-driven approaches [8, 7]. Hu et al., [8] operate under the assumption of pre-availability and disentanglement of causal EVs from observations, using these EVs as suitable subgoals for HRL. However, they overlook cases where these assumptions are not applicable, e.g., the observation is the image. In our approach, subgoals are determined by abstract representations of the observation and action, thereby, extending the applications of causal HRL to unfactorized environments.

3 Methods

3.1 Background

RL Preliminaries.

We are concerned with the Partially Observable Markov Decision Process (POMDP) framework, denoted as the tuple $(S, A, O, P, Z, r, \gamma)$. The framework includes sets of states S , actions A , observations O providing partial information of the true state, a transition probability function $P(s' | s, a)$, and an observation model Z denoted as $Z(o | s, a)$, indicating the probability of observing o when taking action a in state s . $r : S \times A \rightarrow R$ is a reward function that defines the immediate reward that the agent receives for taking an action in a given state, and discount factor γ . The objective of the RL agent is to maximize the expected discounted cumulative reward $E_{\pi, P} [\sum_{t=0}^{\infty} \gamma^t r(s_t, a_t)]$, over a policy function π mapping a state to a distribution over actions.

Causality.

Causality is explored through the analysis of relationships among variables and events [16]. It can be described using the SCM framework [16]. SCM, for a finite set V comprising M variables, is $V_i := f_i(\text{PA}(V_i)_{(G)}, U_i), \forall i \in \{1, \dots, M\}$, where $F = \{f_1, f_2, \dots, f_M\}$ denotes the set of generating functions based on the causal graph G and $U = \{U_1, U_2, \dots, U_M\}$ represents the set of noise in the model. The graph $G = \{V, E\}$ provides the edge $e_{ij} \in E$, representing variable V_i causes on variable V_j , where $e_{ij} = 1$ if $V_j \in \text{PA}(V_i)$, else, $e_{ij} = 0$. The SCM framework can be characterized by two parameter sets: the functional parameter δ , representing the generating function f ; the structural parameter $\eta \in R^{M \times M}$, modelling the adjacency matrix of G [10].

3.2 Variable-Agnostic Causal Exploration Reinforcement Learning Framework

3.2.1 Overview.

The primary argument of VACERL revolves around the existence of a finite set of environment variables (EVs) that the agent should prioritize when constructing the causal graph. We provide a mechanism to detect these variables, aiming to reduce the number of nodes in the causal graph mitigating the complexity of causal discovery. Initially, we deploy an agent to randomly explore the environment and gather successful trajectories. Once the agent accidentally reaches the goal a few times, we initiate Phase 1, reformulating EVs detection into finding the “*crucial observation-action steps*” (*COAS*) from the collected trajectories. The agent is equipped with the ability to rank the importance of these steps by employing the Transformer (*TF*) model’s attention scores (a_s). Top- M highest-score steps will form the crucial set S_{COAS} . Subsequently, in Phase 2, we identify the causal relationships among steps in S_{COAS} to learn the causal graphs G of the environment. In Phase 3, where we extract a hierarchy causal tree from graph G and use it to design two approaches, enhancing the RL agent’s exploration capability. We then utilize the updated agent to gather more successful trajectories and repeat the process from Phase 1. See Fig. 1(c) for an overview of VACERL and detailed implementation in Supp. A ¹.

¹The source is available at <https://github.com/mhngu23/Variable-Agnostic-Causal-Exploration-for-Reinforcement-Learning-VACERL>

3.2.2 Phase 1: Crucial Step Detection.

We hypothesize that important steps (a step is a pair of observation and action) are those in the agent’s memory that the agent must have experienced to reach the goal. Hence, these steps should be found in trajectories where the agent successfully reaches the goal. We collect a buffer $B = (\{o_t^1, a_t^1\}_{t=1}^{T^1}, \{o_t^2, a_t^2\}_{t=1}^{T^2}, \dots, \{o_t^n, a_t^n\}_{t=1}^{T^n})$, where n is the number of episodes wherein the agent successfully reaches the goal state, o_t and a_t is the observation and action, respectively at step t in an episode, and T^k is the number of steps in the k -th episode. We train the TF model, whose input consists of steps from the beginning to the second-to-last step in each episode and the output is the last step. The reasoning behind choosing the last step as the prediction target is that it highlights which steps in the trajectories are crucial for successfully reaching the goal. For a training episode k -th sampled from B , we predict $(\hat{o}_T^k, \hat{a}_T^k) = TF(\{o_t^k, a_t^k\}_{t=1}^{T^k-1})$. The model is trained to minimize the loss $\mathcal{L}_{TF} = \mathbb{E}_k [MSE((o_T^k, a_T^k), (\hat{o}_T^k, \hat{a}_T^k))]$, where MSE is the mean square error. Following training, we rank the significant observation-action steps based on their attention scores a_s (detailed in Supp. A)

and pick out the top- M highest-score steps. We argue that the top-attended steps should cover crucial observations and actions that contribute to the last step prediction task, associated with meaningful causal variables. For instance, observing the key and the action of picking it up are linked to the variable “key”.

In continuous state space, the agent may repeatedly attend to similar steps involving the same variable. For example, the agent might select multiple instances of observing the key, from different positions where the agent is located, and picks it up. As a result, the set $SCOAS$ will be filled with similar steps relating to picking up the key and ignoring other important steps. To address this, we introduce a function `is_sim` to decide if two steps are the same:

- For discrete action space environments, $\text{is_sim}((o, a), (o', a')) = 1$ if $\cos(o, o') > \phi_{\text{sim}}$ and $a = a'$, else 0.
- For continuous action space environments, $\text{is_sim}((o, a), (o', a')) = 1$ if $\cos((o, a), (o', a')) > \phi_{\text{sim}}$, else 0.

where $\text{Cos}(o, o') = \frac{o \cdot o'}{\|o\| \cdot \|o'\|}$ and ϕ_{sim} is a similarity threshold. Intuitively, if the agent has two observations with a high cosine similarity and takes the same action, these instances are grouped. The score a_s for a group is the highest a_s among the steps in this group. The proposed `is_sim` method will also be effective in noisy environments, particularly when the observations are trained representations rather than raw pixel data. Subsequently, we add the steps with the highest a_s to $SCOAS$. We define an abstract function \mathcal{I} to map a pair (o_t^k, a_t^k) to an element i in $SCOAS$: $i = \mathcal{I}((o_t^k, a_t^k)) \iff \text{is_sim}((o_t^k, a_t^k), (o, a)_i) = 1$ and collect a new buffer B^* , where:

$$B^* = B \setminus \left\{ (o_t^k, a_t^k) : \mathcal{I}((o_t^k, a_t^k)) \notin SCOAS \right\} \quad (1)$$

Here, B^* is B removing steps that are unimportant (not in $SCOAS$).

3.2.3 Phase 2: Causal Structure Discovery.

Inspired by the causal learning method proposed by Ke et al., [10], we uncover the causal relationships among M steps identified in the $SCOAS$ set. Our approach optimizes the functional parameter δ and the structural parameter η associated with the SCM framework. The optimization of these parameters follows a two-phase iterative update process, wherein one parameter is

fixed while the other is updated. Both sets of parameters are initialized randomly and undergo training using the buffer B^* (Eq. 1). Our intuition for training the SCM is that the ‘‘cause’’ step has to precede its ‘‘effect’’ step. Therefore, we train the model to predict the step at timestep t using the sequence of steps leading to that particular timestep.

In the first causal discovery phase, we fix η and optimize δ . For a step t in the trajectory k -th, we formulate f as:

$$(\hat{o}_t^k, \hat{a}_t^k) = f_{\delta, \mathcal{I}((o_t^k, a_t^k))}(\{o_{t'}^k, a_{t'}^k\}_{t'=1}^{t-1} \wedge (\mathcal{I}(o_{t'}^k, a_{t'}^k)) \in \text{PA}(\mathcal{I}(o_t^k, a_t^k)) | G) \quad (2)$$

where $\{o_{t'}^k, a_{t'}^k\}_{t'=1}^{t-1}$ is the sequence of steps from 1 to $t - 1$ that belong to the parental set of $\text{PA}(\mathcal{I}(o_t^k, a_t^k))$, as defined by the current state of G parameterized by η . We use MSE as the loss function:

$$\mathcal{L}_{\delta, G} = \mathbb{E}_{t, k} \left[\text{MSE} \left((o_t^k, a_t^k), (\hat{o}_t^k, \hat{a}_t^k) \right) \right] \quad (3)$$

In the second phase, we fix δ and optimize the parameter η by updating the causality from variable X_j to X_i as $\eta_{ij} = \eta_{ij} - \beta \sum_h \left((\sigma(\eta_{ij}) - e_{ij}^{(h)}) \mathcal{L}_{\delta, G^{(h)}, i}(X) \right)$, where h indicates the h -th drawn sample of causal graph G , given the current parameter η , and β is the update rate. $e_{ij}^{(h)}$ is the edge from variable X_j to X_i of $G^{(h)}$, and σ is the sigmoid function. $\mathcal{L}_{\delta, G^{(h)}, i}(X)$ is the MSE loss in Eq. 3 for specific variable X_i of current function f_{δ, X_i} under graph $G^{(h)}$. After updating parameter η for a number of steps, we repeat the optimization process of parameter δ . Finally, we use the resulting structural parameter η to construct the causal graph G . We derive edge e_{ij} of graph G , using:

$$e_{ij} = \begin{cases} 1 & \text{if } \eta_{ij} > \eta_{ji} \text{ and } \sigma(\eta_{ij}) > \phi_{causal} \\ 0 & \text{otherwise} \end{cases} \quad (4)$$

where ϕ_{causal} is the causal threshold.

3.2.4 Phase 3: Agent Training with Causal Information.

We extract a refined hierarchy causal tree from graph G with an intuition to focus on steps that are relevant to achieving the goal. Using the goal-reaching step as the root node of the tree, we recursively determine the parental steps of this root node within graph G , and subsequently for all identified parental steps. This causal tree is used to design causal exploration approaches. These approaches include (i) intrinsic rewards based on the causal tree, and (ii) utilizing causal nodes as subgoals for HRL. For the first approach, we devise a reward function where nodes closer to the root are deemed more important and receive higher rewards, preserving the significance of the reward associated with the root node and maintaining the agent’s focus on the goal. In the second approach, subgoals are sampled from nodes in the causal tree, with nodes closer to the root sampled more frequently. We present the detailed implementations and empirically evaluate these approaches in Sec. 4.1 and Sec. 4.2.

4 Experiments

4.1 VACERL: Causal Intrinsic Rewards - Implementation and Evaluation

Causal Intrinsic Reward.

To establish the relationship where nodes closer to the goal hold greater importance, while ensuring the agent remains focused on the goal, we introduce intrinsic reward formulas as follows:

$$r_{causal}(o, a) = r_g - (d - 1)r_0 \quad \forall (o, a) \in D_d \quad (5)$$

where r_g is the reward given when the agent reach the goal, $r_{causal}(o, a)$ is the intrinsic reward given to a node (o, a) , D_d is the set of nodes at depth d of the tree, $r_0 = \alpha(r_g/h)$ with α is a hyperparameter and h is the tree height. In the early learning stage, especially for hard exploration environments, the causal graph may not be well defined and thus, r_{causal} may not provide a good incentive. To mitigate this issue, we augment r_{causal} with a count-based intrinsic reward, aiming to accelerate the early exploration stage. Intuitively, the agent is encouraged to visit never-seen-before observation-action pairs in early exploration. Notably, unlike prior count-based methods [2], we restrict counting to steps in S_{COAS} , i.e., only crucial steps are counted. Our final intrinsic reward is:

$$r_{causal}^+ = \left(1/\sqrt{n_{(o,a)_t}}\right) r_{causal}(o_t, a_t) \quad (6)$$

where $n_{(o,a)_t}$ is the number of time observation o and action a is encountered up to time step t . Starting from zero, this value increments with each subsequent encounter. We add the final intrinsic reward to the environment reward to train the policy. The total reward is $r(s_t, a_t) = r_{env}(s_t, a_t) + r_{causal}^+(s_t, a_t)$, where r_{env} is the extrinsic reward provided by the environment.

Environments.

We perform experiments across three sets of environments: FrozenLake (FL), Minihack (MH), and Minigrid (MG). These environments are tailored to evaluate the approach in sparse reward settings, where the agent receives a solitary +1 reward upon achieving the goal (detailed in Supp. B)

FL includes the 4x4 (4x4FL) and 8x8 (8x8FL) FrozenLake environments (Supp Fig. B.1(d,e)) [27]. Although these are classic navigation problems, hidden causal relationships exist between steps. The pathway of the agent can be conceptualized as a causal graph, where each node represents the agent’s location cell and its corresponding action. For example, moving right from the cell on the left side of the lake can be identified as the cause of the agent falling into the lake cell. We use these environments to test VACERL’s efficiency in discrete state space, where `is_sim` is not used.

MH includes MH-1 (Room), MH-2 (Room-Monster), MH-3 (Room-Ultimate) and MH-4 (River-Narrow) [20]. These environments pose harder exploration challenges compared to FL due to the presence of more objects. Some environments even require interaction with these objects to reach the goal, such as killing monsters (MH-2 and MH-3) or building bridges (MH-4). For this set of environments, we use pixel observations.

MG is designed based on Minigrid Environment [4], with escalating causality levels. These include the Key Corridor (MG-1) (Supp. Fig. B.1(a)) and 3 variants of the BlockUnlockPickUp:

2 2x2 rooms (MG-2 Fig. 1(a)), 2 3x3 rooms (MG-3) and the 3 2x2 rooms (MG-4) (Supp Fig. B.1(b,c)). The task is to navigate and locate the goal object, in a different room. These environments operate under POMDP, enabling us to evaluate the framework’s ability to construct the causal graph when only certain objects are observable at a timestep. In these environments, the agent completes the task by following the causal steps: firstly, remove the obstacle blocking the door by picking it up and dropping it in another position, then, pick up the key matching the colour of the door to open it; and finally, pick up the blue box located in the rightmost room, which is the goal. In MG-3, distracting objects are introduced to distract the agent from this sequence of action. In any case, intrinsic exploration motivation is important to navigate due to reward sparsity; however, blind exploration without an understanding of causal relationships can be ineffective.

Noisy-TV setting is implemented as an additional action (action to watch TV) and can be incorporated into any of the previous environments, so the agent has the option to watch the TV at any point while navigating the map [12]. When taking this watching TV action, the agent will be given white noise observations sampled from a standard normal distribution. As sampled randomly, the number of noisy observations can be conceptualized as infinite.

Baselines.

PPO [21], a policy gradient method, serves as the backbone algorithm of our method and other baselines. Following Schulman et al., [21], vanilla PPO employs a simple entropy-based exploration approach. Other baselines are categorized into causal and non-causal intrinsic motivation. Although our focus is causal intrinsic reward, we include non-causal baselines for comprehensiveness. These include popular methods: Count-based [2, 26] and RND [3]. Causal motivation baselines include ATTENTION and CAI, which are two methods that have been used to measure causal influence [22, 18]. We need to adapt these methods to follow our assumption of not knowing causal variables. The number of steps used to collect initial successful trajectories and to reconstruct the causal graph (denoted as H_s and T_s respectively) for VACERL and causal baselines are provided for each environment in Supp. D. However, not all causal methods can be adapted, and as such, we have not conducted comparisons with approaches, such as [8]. Additionally, as we do not require demonstrating trajectory from experts, we do not compare with causal imitation learning methods [6, 24].

Results.

In this section, we present our empirical evaluation results of VACERL with causal intrinsic rewards.

Discrete State Space: Table 1 illustrates that our rewards improve PPO’s performance by approximately 30%, in both 4x4FL and 8x8FL environments. Notably, VACERL outperforms both causal baselines, ATTENTION and CAI. Specifically, VACERL surpasses ATTENTION by 67% and 39% in 4x4FL and 8x8FL. CAI fails to learn the tasks within the specified steps due to insufficient trajectories in the agent’s memory for precise causality estimation between all steps. In contrast, our method, incorporating a crucial step detection phase, requires fewer trajectories to capture meaningful causal relationships in the environment. VACERL also performs better than Count-based by 66% in 4x4FL and 100% in 8x8FL, and RND by 51% in 4x4FL and 31% in 8x8FL. We hypothesize that Count-based and RND’s intrinsic rewards are unable to encourage the agent to avoid the trapping lakes, unlike VACERL’s are derived from only successful

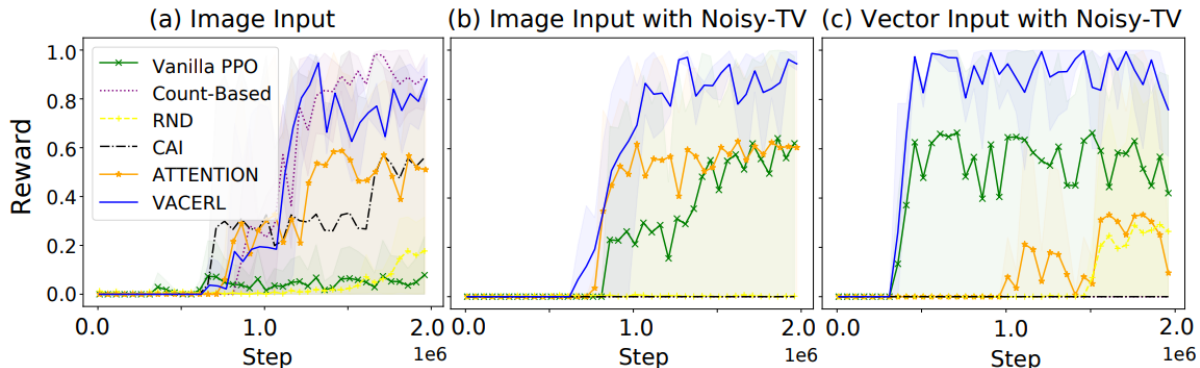


Figure 2: The learning curves for MG-2 illustrate the average return (mean \pm std over 3 runs) of 50 testing episodes over 2 million training steps. For VACERL and causal baselines, the learning curves include 300,000 steps dedicated to the initial random exploration period to collect initial successful trajectories, with rewards for each step set to 0. The causal graph is reconstructed every 300,000 steps.

trajectories promoting safer exploration.

MG-2 Learning Curve Analysis: We conduct experiments with 2 types of observation space (image and vector) and visualize the learning curves in Fig. 2(a) and Supp. Fig. B.4. Results demonstrate that VACERL outperforms vanilla PPO, causal baselines, and RND in both types of observation space. While VACERL shows slightly slower progress than Count-based in early steps, it quickly catches up in later stages, ultimately matching optimal performance. We attribute this to VACERL requires a certain number of training steps to accurately acquire the causal graph before the resulting causal rewards influence the agent’s training—a phenomenon observed in other causal baselines as well.

Continuous State Space: Table 1 summarizes the testing results on 8 continuous state space environments (MH-1 to MG-4). In most of these environments, VACERL demonstrates superior performance. It only ranks as the second-best in MH-4, MG-1 and MG-2 with competitive returns. In MG-3 environment, at 30 million steps, VACERL achieves the best result with an average return of 0.77, outperforming the second-best Count-based by 10%, while other baselines show little learning. Notably, in the hardest task MG-4, only VACERL can show signs of learning, achieving an average score of 0.29 after 50 million steps whereas other baselines’ returns remain zero. Additional learning curves and results are provided in Supp. B.

Under Noisy-TV: Fig. 2(b, c), showing the results on MG-2 environment under Noisy-TV setting, confirm that our reward exhibits greater robustness in Noisy-TV environments compared to traditional approaches. Count-based, CAI, and RND fail in this setting as they cannot differentiate noise from meaningful novelty, thus, getting stuck watching Noisy-TV. While the noise less impacts ATTENTION and naive PPO, their exploration strategies are not sufficient for sparse reward environments. Overall, VACERL is the only method performing well across all settings, with or without Noisy-TV.

Task	Step (,000)	PPO	Count-Based	RND	ATTENTION	CAI	VACERL
4x4FL	5	66 ± 47	33 ± 57	48 ± 50	32 ± 56	0 ± 0	97 ± 4
8x8FL	35	66 ± 58	0 ± 0	66 ± 57	59 ± 53	0 ± 0	96 ± 4
MH-1	5	66 ± 57	99 ± 0	88 ± 20	66 ± 57	33 ± 57	99 ± 0
MH-2	1,000	77 ± 7	71 ± 11	68 ± 3	76 ± 15	67 ± 13	85 ± 8
MH-3	1,000	61 ± 8	67 ± 3	61 ± 8	65 ± 3	62 ± 7	68 ± 10
MH-4	5,000	42 ± 3	47 ± 7	42 ± 6	42 ± 3	45 ± 4	46 ± 3
MG-1	500	82 ± 2	85 ± 12	85 ± 12	98 ± 2	66 ± 57	94 ± 1
MG-2	2,000	9 ± 13	94 ± 4	20 ± 16	48 ± 43	59 ± 51	90 ± 14
MG-3	30,000	0 ± 0	69 ± 25	11 ± 6	26 ± 46	0 ± 0	77 ± 3
MG-4	50,000	0 ± 0	0 ± 0	0 ± 0	0 ± 0	0 ± 0	29 ± 50

Table 1: FL, MH and MG: Average return ($\times 100$) of 50 episodes (mean \pm std. over 3 runs). Bold denotes the best results. For VACERL and causal baselines (CAI and ATTENTION). Steps include the initial steps, as detailed in Supp. D, dedicated to collecting initial successful trajectories.

4.2 VACERL: Causal Subgoals - Implementation and Evaluation

Causal subgoals sampling.

In HRL, identifying subgoals often relies on random exploration [13, 31], which can be inefficient in large search spaces. We propose leveraging causal nodes as subgoals, allowing agents to actively pursue these significant nodes. To incorporate causal subgoals into exploration, we suggest substituting a portion of the random sampling with causal subgoal sampling. Specifically, in the HRL method under experimentation where subgoals are randomly sampled 20% of the time, we replace a fraction of this 20% with a node from the causal tree as a subgoal, while retaining random subgoals for the remainder. Eq. 7 denotes the probability of sampling a node i at depth $d > 0$ (excluding the root node as this is the ultimate goal) from the causal tree:

$$P^{(i)} = (d_i)^{-1} / \sum_{i=1}^N (d_i)^{-1} \quad (7)$$

with d_i is the depth of node i and N is the number of nodes in the causal tree.

Environments.

We use FetchReach and FetchPickAndPlace environments from Gymnasium-Robotics [11]. These are designed to test goal-conditioned RL algorithms. We opt for sparse rewards settings, in which only a single reward of 0 is given if the goal is met, otherwise -1 (detailed in Supp. C).

Baselines.

HAC [13], a goal-conditioned HRL algorithm, serves as the backbone and a baseline. HAC is implemented as a three-level DDPG [14] with Hindsight Experience Replay (HER) [1], where the top two levels employ a randomized mechanism for subgoal sampling. We also evaluate our performance against the standard DDPG+HER algorithm [1] on the FetchPickAndPlace environment, as this is the more challenging task [19] and for comprehensiveness.

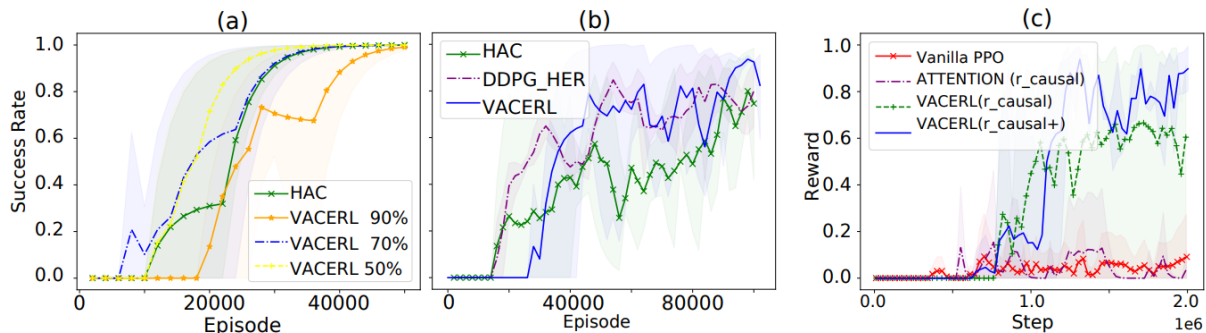


Figure 3: **(a, b)**: Learning curves of FetchReach (a) (% represents the portion of random subgoals replaced) and FetchPickAndPlace (b). The average return of 50 testing episodes (mean \pm std over 3 runs). For VACERL, successful trajectories are collected during training and causal graphs are reconstructed every 2,000 episodes and 10,000 episodes, respectively. **(c)**: Component contribution study on MG-2 task. The average return of 50 episodes (mean \pm std. over 3 runs).

Results.

In this section, we outline our empirical evaluation results of VACERL with causal subgoals.

FetchReach: We assess the impact of replacing varying proportions of random sampling subgoals with nodes from the causal graph, based on Eq. 7, on the performance of the HRL agent. The learning curve in Fig. 3(a) suggests that replacing with percentages of 50% and 70% enhances the sample efficiency of the Vanilla HAC. Notably, when employing a 70% substitution rate, agents demonstrate signs of learning after only 4,000 episodes, a considerable improvement over the HAC agent’s 10,000 episodes. Conversely, replacing 50% leads to a swifter convergence, at 20,000 episodes comparing to HAC at 25,000 episodes. Additional experiments (Supp. C) demonstrate that this accelerated convergence rate is attributable to the learned causal subgoals. In contrast, employing a 90% substitution rate results in a decline in performance. We assert that this decline comes from insufficient exploration of new subgoals, leading to an inadequate number of trajectories in buffer B for causal discovery.

FetchPickAndPlace: We adopt the 50% replacement, which yielded the most stable performance in the FetchReach environment for this environment. The learning curve of VACERL in Fig. 3(b) shows a similar pattern to the learning curves for the MG-2 task in Fig. 2(a). VACERL progresses slower but eventually achieves optimal performance, surpassing DDPG+HER and HAC after 90,000 episodes. In this environment, we reconstruct the causal tree every 10,000 episodes, and as seen in the learning curve, the RL agent’s performance begins to improve after approximately 20,000 episodes (worst case improves after 40,000 episodes).

4.3 Ablation Study and Model Analysis

We use MG-2 (Fig. 1(a)) task and causal intrinsic reward for our analysis.

Crucial Step Detection Analysis: We investigate how the the Transformer model TF ’s performance changes with varying buffer B sizes. As depicted in Fig. 4(a,b), increasing the number of trajectories in B enhances the framework’s accuracy in detecting important steps through attention. Initially, with 4 trajectories (Fig. 4(a)), TF attends to all actions in the top-left grid. However, after being trained with 40 trajectories (Fig. 4(b)), TF correctly attends to pick-up

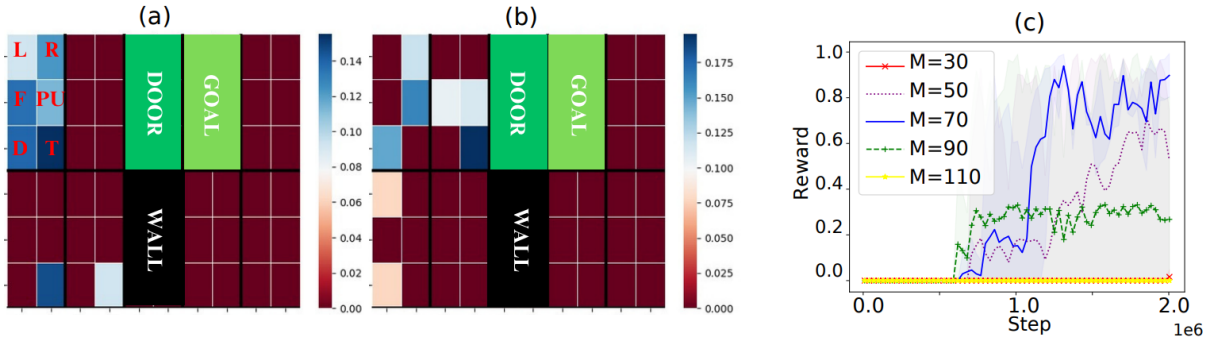


Figure 4: **(a,b)**: Attention heatmap when B has 4 (a) and 40 (b) trajectories for MG-2 task. We highlight the top-8 attended actions and their grids. A big cell (black boundary) represents a grid in the map, containing smaller cells representing 6 possible actions. **(c)**: Results tuning the number of steps (M) in $SCOAS$. Average return of 50 episodes (mean \pm std. over 3 runs).

action (PU) in the top-left grid, corresponding to the key pickup event. It can also attend to toggle action (T) in front of the door, corresponding to using the key to open the door. Additional visualization for 4x4FL is in Supp. Fig. B.6.

Next, we investigate the effects of employing varying sizes of $SCOAS$ (M). The results in Fig. 4(c) reveal that varying M changes the performance of the agent drastically. If M is too small, the agent will not be able to capture all causal relations, thereby failing to mitigate the issue of sparse reward. On the other hand, too large M can be noisy for the causal discovery phase as the causal graph will have redundant nodes. We find that the optimal value for M , in MG-2, is 70, striking a balance between not being too small or too large.

Intrinsic Reward Shaping Analysis: We exclude the counting component (Eq. 6) from the final intrinsic reward to assess the agent’s exploration ability simply based on r_{causal} . The results in Fig. 3(c) show that the agent remains proficient relying only on the causally motivated reward (green curve). In particular, in the absence of Eq. 6, the VACERL agent still outperforms Vanilla PPO. However, its performance is not as optimal as the full VACERL (r_{causal}^+ , blue curve). This is because, in early iteration, the causal graph is not yet well defined, diminishing the efficiency of solely using the causal intrinsic reward r_{causal} .

Causal Structure Discovery Contribution: We study the contribution of Phase 2, comparing between causality and attention correlation. We directly used the a_s assigned to each (o, a) in Phase 1 to compute the intrinsic reward: $r_{bonus}(o, a) = \alpha a_s(o, a)$, where α is the hyperparameter in Eq. 5. This reward differs from the ATTENTION reward used in Sect. 4.1 in that the augmentation in Eq. 6 is not applied. We expect that as attention score is a reliable indicator of correlation, building intrinsic reward upon it would benefit the agent, albeit not as effectively as when a causal graph is used (correlation is not as good as causality). The learning curve in Fig. 3(c) showcases that the result using causal as intrinsic motivation (green curve) performs better than using attention correlation (purple curve) by a large margin. To further evaluate, we extract the learned causal graph in Fig. 5 and present the detailed analysis of this graph in Supp. B. The result shows that our method can recover an approximation of the ground truth causal graph. Although there are redundant nodes and edges, important causal hierarchy is maintained, e.g., “open door” is the parental step of “pickup key”.

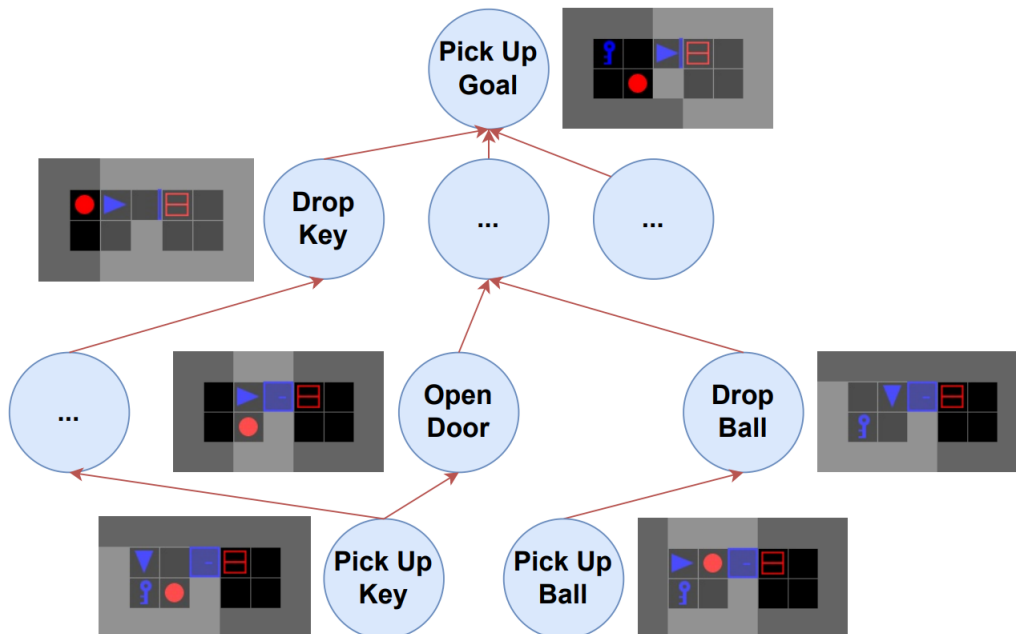


Figure 5: Causal graph that was generated as a result of the algorithm for MG-2. The RGB images display the agent’s viewports during the execution of the corresponding actions.

5 Conclusion

This paper introduces VACERL, a framework that enhances RL agent performance by analyzing causal relationships among agent observations and actions. Unlike previous methods, VACERL addresses causal discovery without assuming specified causal variables, making it applicable to variable-agnostic environments. Understanding these causal relationships becomes crucial for effective agent exploration, particularly in environments with complex causal structures or irrelevant actions, such as the Noisy-TV problem. We propose two methods to leverage the identified causal structure. Future research could explore other methods utilizing this structure. Empirical evaluations in sparse reward navigation and robotic tasks demonstrate the superiority of our approach over baselines. However, a limitation is the introduction of new hyperparameters, which require adjustment for different settings.

References

- [1] Andrychowicz, M., Wolski, F., Ray, A., Schneider, J., Fong, R., Welinder, P., McGrew, B., Tobin, J., Pieter Abbeel, O., Zaremba, W.: Hindsight experience replay. *Advances in neural information processing systems* **30** (2017)
- [2] Bellemare, M., Srinivasan, S., Ostrovski, G., Schaul, T., Saxton, D., Munos, R.: Unifying count-based exploration and intrinsic motivation. *Advances in neural information processing systems* **29** (2016)
- [3] Burda, Y., Edwards, H., Storkey, A., Klimov, O.: Exploration by random network distillation. *arXiv preprint arXiv:1810.12894* (2018)

- [4] Chevalier-Boisvert, M., Dai, B., Towers, M., de Lazcano, R., Willems, L., Lahlou, S., Pal, S., Castro, P.S., Terry, J.: Minigrid & miniworld: Modular & customizable reinforcement learning environments for goal-oriented tasks. *CoRR* **abs/2306.13831** (2023)
- [5] Corcoll, O., Vicente, R.: Disentangling causal effects for hierarchical reinforcement learning. *arXiv preprint arXiv:2010.01351* (2020)
- [6] De Haan, P., Jayaraman, D., Levine, S.: Causal confusion in imitation learning. *Advances in neural information processing systems* **32** (2019)
- [7] Ding, W., Lin, H., Li, B., Zhao, D.: Generalizing goal-conditioned reinforcement learning with variational causal reasoning. *Advances in Neural Information Processing Systems* **35**, 26532–26548 (2022)
- [8] Hu, X., Zhang, R., Tang, K., Guo, J., Yi, Q., Chen, R., Du, Z., Li, L., Guo, Q., Chen, Y., et al.: Causality-driven hierarchical structure discovery for reinforcement learning. *Advances in Neural Information Processing Systems* **35**, 20064–20076 (2022)
- [9] Hung, C.C., Lillicrap, T., Abramson, J., Wu, Y., Mirza, M., Carnevale, F., Ahuja, A., Wayne, G.: Optimizing agent behavior over long time scales by transporting value. *Nature communications* **10**(1), 5223 (2019)
- [10] Ke, N.R., Bilaniuk, O., Goyal, A., Bauer, S., Larochelle, H., Schölkopf, B., Mozer, M.C., Pal, C., Bengio, Y.: Learning neural causal models from unknown interventions. *arXiv preprint arXiv:1910.01075* (2019)
- [11] de Lazcano, R., Andreas, K., Tai, J.J., Lee, S.R., Terry, J.: *Gymnasium robotics* (2023), <http://github.com/Farama-Foundation/Gymnasium-Robotics>
- [12] Le, H., Do, K., Nguyen, D., Venkatesh, S.: Beyond surprise: Improving exploration through surprise novelty. In: *Proceedings of the 23rd International Conference on Autonomous Agents and Multiagent Systems*. p. 1084–1092. *AAMAS '24, International Foundation for Autonomous Agents and Multiagent Systems, Richland, SC* (2024)
- [13] Levy, A., Konidaris, G., Platt, R., Saenko, K.: Learning multi-level hierarchies with hindsight. *arXiv preprint arXiv:1712.00948* (2017)
- [14] Lillicrap, T.P., Hunt, J.J., Pritzel, A., Heess, N., Erez, T., Tassa, Y., Silver, D., Wierstra, D.: Continuous control with deep reinforcement learning. *arXiv preprint arXiv:1509.02971* (2015)
- [15] Mnih, V., Kavukcuoglu, K., Silver, D., Rusu, A.A., Veness, J., Bellemare, M.G., Graves, A., Riedmiller, M., Fidjeland, A.K., Ostrovski, G., et al.: Human-level control through deep reinforcement learning. *nature* **518**(7540), 529–533 (2015)
- [16] Pearl, J.: *Causal inference in statistics: An overview* (2009)
- [17] Pitis, S., Chan, H., Zhao, S., Stadie, B., Ba, J.: Maximum entropy gain exploration for long horizon multi-goal reinforcement learning. In: *International Conference on Machine Learning*. pp. 7750–7761. *PMLR* (2020)

- [18] Pitis, S., Creager, E., Garg, A.: Counterfactual data augmentation using locally factored dynamics. *Advances in Neural Information Processing Systems* **33**, 3976–3990 (2020)
- [19] Plappert, M., Andrychowicz, M., Ray, A., McGrew, B., Baker, B., Powell, G., Schneider, J., Tobin, J., Chociej, M., Welinder, P., et al.: Multi-goal reinforcement learning: Challenging robotics environments and request for research. *arXiv preprint arXiv:1802.09464* (2018)
- [20] Samvelyan, M., Kirk, R., Kurin, V., Parker-Holder, J., Jiang, M., Hambro, E., Petroni, F., Kuttler, H., Grefenstette, E., Rocktäschel, T.: Minihack the planet: A sandbox for open-ended reinforcement learning research. In: *Thirty-fifth Conference on Neural Information Processing Systems Datasets and Benchmarks Track (Round 1)* (2021), <https://openreview.net/forum?id=skFwlyefkWJ>
- [21] Schulman, J., Wolski, F., Dhariwal, P., Radford, A., Klimov, O.: Proximal policy optimization algorithms. *arXiv preprint arXiv:1707.06347* (2017)
- [22] Seitzer, M., Schölkopf, B., Martius, G.: Causal influence detection for improving efficiency in reinforcement learning. *Advances in Neural Information Processing Systems* **34**, 22905–22918 (2021)
- [23] Silver, D., Schrittwieser, J., Simonyan, K., Antonoglou, I., Huang, A., Guez, A., Hubert, T., Baker, L., Lai, M., Bolton, A., et al.: Mastering the game of go without human knowledge. *nature* **550**(7676), 354–359 (2017)
- [24] Sun, Z., He, B., Liu, J., Chen, X., Ma, C., Zhang, S.: Offline imitation learning with variational counterfactual reasoning. *Advances in Neural Information Processing Systems* **36** (2023)
- [25] Sutton, R.S., Barto, A.G.: *Reinforcement learning: An introduction*. MIT press (2018)
- [26] Tang, H., Houthoofd, R., Foote, D., Stooke, A., Xi Chen, O., Duan, Y., Schulman, J., DeTurck, F., Abbeel, P.: # exploration: A study of count-based exploration for deep reinforcement learning. *Advances in neural information processing systems* **30** (2017)
- [27] Towers, M., Terry, J.K., Kwiatkowski, A., Balis, J.U., Cola, G.d., Deleu, T., Goulão, M., Kallinteris, A., KG, A., Krimmel, M., Perez-Vicente, R., Pierré, A., Schulhoff, S., Tai, J.J., Shen, A.T.J., Younis, O.G.: *Gymnasium* (Mar 2023). <https://doi.org/10.5281/zenodo.8127026>, <https://zenodo.org/record/8127025>
- [28] Vaswani, A., Shazeer, N., Parmar, N., Uszkoreit, J., Jones, L., Gomez, A.N., Kaiser, Ł., Polosukhin, I.: Attention is all you need. *Advances in neural information processing systems* **30** (2017)
- [29] Zeng, Y., Cai, R., Sun, F., Huang, L., Hao, Z.: A survey on causal reinforcement learning. *arXiv preprint arXiv:2302.05209* (2023)
- [30] Zhang, P., Liu, F., Chen, Z., Jianye, H., Wang, J.: Deep reinforcement learning with causality-based intrinsic reward (2020)
- [31] Zhang, T., Guo, S., Tan, T., Hu, X., Chen, F.: Generating adjacency-constrained subgoals in hierarchical reinforcement learning. *Advances in Neural Information Processing Systems* **33**, 21579–21590 (2020)

- [32] Zhang, Y., Du, Y., Huang, B., Wang, Z., Wang, J., Fang, M., Pechenizkiy, M.: Interpretable reward redistribution in reinforcement learning: A causal approach. *Advances in Neural Information Processing Systems* **36** (2024)
- [33] Todorov, E., Erez, T., Tassa, Y.: Mujoco: A physics engine for model-based control. In: 2012 IEEE/RSJ international conference on intelligent robots and systems. pp. 5026–5033. IEEE (2012)

A Details of Methodology

A.1 VACERL Framework

The detailed processing flow of the VACERL framework is described in Algo. 1. Buffer B is initialized using the process from lines 2-6, using a random policy to collect successful trajectories (Note: as long as the agent can accidentally reach the goal and add 1 trajectory to B , we can start the improving process). We, then, start our iterative process (the outer loop). In Phase 1, ‘‘Crucial Step Detection’’ (lines 8-21), the process commences with the training of the Transformer model TF using Algo. 2. Subsequently, we collect the dictionary D that maps (o_t^k, a_t^k) to attention score a_s . D is sorted based on a_s . We, then, define `is_sim` function (line 9) and abstract function \mathcal{I} (line 10) to handle similar observation-action steps, and add the top M (o_t^k, a_t^k) steps to the set S_{COAS} using the process from lines 12-20. After collecting S_{COAS} , we apply Eq. 1 to acquire the new buffer B^* . With buffer B^* , we initiate Phase 2 (line 22) called ‘‘Causal Structure Discovery’’. We optimize the two parameters δ and η using Algo. 3 and collect the causal graph G . Using graph G , we collect the causal tree relative to the goal-reaching step to create a hierarchy of steps. We use this hierarchy to calculate the intrinsic reward associated with (o, a) using Eq. 6 or to calculate subgoals sampling probability using Eq. 7. Finally, we train the policy π_θ and adding new successful trajectories to buffer B , summarizing Phase 3 (lines 23-29) called ‘‘Agent Training with Causal Information’’. The process starts again from Phase 1 using the updated buffer B .

A.2 Transformer Model Training

Detailed pseudocode for training the Transformer model is provided in Algo. 2. We utilize the Transformer architecture implemented in PyTorch², for our TF model implementation. This implementation follows the architecture presented in the paper [28], thus, the attention score a_s for a step is computed using the self-attention equation: $\text{softmax}\left(\frac{QK^T}{\sqrt{d_k}}\right)$, where $Q = XW_Q$ represents the query vector, $K = XW_K$ represents the key vector, X is the learned embedding of a step (o_t^k, a_t^k) , and W_Q, W_K are trainable weights. The values of a_s are extracted from the encoder layer of the TF model during the last training iteration. We use a step (o_t^k, a_t^k) as the key in dictionary D that maps to an associated a_s , described in the process in lines 5-11 (Algo. 2).

A.3 SCM Training

The detailed pseudocode is provided in Algo. 3. Our approach involves a two-phase iterative update process, inspired by the causal learning method proposed by Ke et al., [10]. This process optimizes two parameters: the functional parameter δ of generating function f and the structural parameter η of graph G , representing a Structural Causal Model (SCM). In Phase 1 of the process, we want to keep the structural parameter η fixed and update the functional parameter δ , whereas in Phase 2, we keep δ fixed and update η . Both sets of parameters underwent training using the buffer B^* (Eq. 1). The generating function f is initialized as a 3-layer MLP neural

²<https://pytorch.org/docs/stable/generated/torch.nn.Transformer.html>

network with random parameter δ . The parameter $\eta \in R^{M \times M}$, the soft adjacency matrix of size $M \times M$ representing the direct causality graph of the M steps, is initialized as a random $M \times M$ tensor, such that η_{ij} denotes the causal relationship between step at index j of $SCOAS$ on step at index i of $SCOAS$. At each step in lines 4 and 20 of Algo. 3, we sample a hypothesis causal graph G by Bernoulli sampling $Ber((\sigma(\eta)))$ that will be used for the optimization process, where $\sigma(x) = \frac{1}{1+e^{-x}}$.

The intuition behind this optimization process is that the step representing the "cause" should occur before its associated "effect" step, so, for a step t in the trajectory k -th, we formulate f as:

$$(\hat{o}_t^k, \hat{a}_t^k) = f_{\delta, \mathcal{I}(o_t^k, a_t^k)}(\{o_{t'}^k, a_{t'}^k\}_{t'=1}^{t-1}) \wedge (\mathcal{I}(o_{t'}^k, a_{t'}^k) \in \text{PA}(\mathcal{I}(o_t^k, a_t^k)) | G)$$

In our implementation, every steps from 1 to $t-1$ that do not belong to the parental set of $\text{PA}(\mathcal{I}(o_t^k, a_t^k))$ are masked out when inputting into the MLP, in this way, only steps that belong to the parental set of $\text{PA}(\mathcal{I}(o_t^k, a_t^k))$ are used in the prediction of (o_t^k, a_t^k) . To learn f and optimize parameter δ , we compute an MSE loss as denoted in Eq. 3.

In the second phase, we fix δ and optimize the parameter η by updating the causality from variable X_j to X_i . After updating parameter η for several steps, we return to the optimization process of parameter δ .

Finally, we use the resulting structural parameter η to construct the final causal graph G . We first get edge e_{ij} using Eq. 4, where, ϕ_{causal} represents the causal confident threshold. In our implementation, ϕ_{causal} was tuned with the values in $[0.5, 0.6, 0.7, 0.8, 0.9, 1.0]$. This Eq. 4 is used to ensure that there is no internal loop in the adjacency matrix.

A.4 Causal Tree Extraction

We extract a tree from the resultant causal graph G , focusing on the steps relevant to achieving the goal. We use the goal-reaching step as the root of the tree and recursively determine the parental steps of this root node within graph G and add them to the causal tree as new nodes, and subsequently, we will determine the parental steps for all these identified nodes. However, to avoid cycles in the tree, we need to add an order of ranking, thus, we use the ranking of attention score a_s . So, for edge e_{ij} from variable X_i to variable X_j , we will remove the edge e_{ij} if a_s of X_i is smaller than the a_s of X_j , even if $e_{ij}=1$ according to the graph G .

B Setting to Test VACERL Causal Intrinsic Reward

B.1 Environments

FrozenLake Environments

These tasks involve navigating the FrozenLake environments of both 4x4 (4x4FL) and 8x8 (8x8FL) [27]. Visualizations for these environments can be found in Fig. B.1(d,e). The goal of the agent involves crossing a frozen lake from the starting point located at the top-left corner of the map to the goal position located at the bottom-right corner of the map without falling

into the frozen lake. The observation in these environments is a value representing the current position of the agent. The number of possible positions depends on the map size, with 4x4FL having 16 positions and 8x8FL having 64 positions. The agent is equipped with four discrete actions determining the direction of the agent’s movement [27]. If the agent successfully reaches the goal, it receives a +1 reward. However, if it falls into the lake or fails to reach the goal within a predefined maximum number of steps, it receives a 0 reward. The chosen maximum number of steps for 4x4FL and 8x8FL to validate our framework are 100 steps and 2000 steps, respectively.

Minihack Environments

These tasks involve MH-1 (MiniHack-Room-5x5-v0), MH-2 (MiniHack-Room-Monster-5x5-v0), MH-3 (MiniHack-Room-Ultimate-5x5-v0) and MH-4 (MiniHack-River-Narrow-v0); a suit of environments collected from [20]. These environments present more challenging exploration scenarios compared to FrozenLake environments due to the increased number of objects. Certain environments necessitate interaction with objects to achieve the goal, such as defeating monsters (MH-2 and MH-3) or constructing bridges (MH-4). If the agent successfully reaches the goal within a predefined maximum number of steps, it receives a +1 reward; otherwise, it receives a 0 reward. The maximum number of steps for all four environments is the default number of steps in [20].

Minigrid Environments

These tasks involve four environments: Key Corridor (MG-1 Fig. B.1(a)), two 2x2 rooms (MG-2 Fig. 1), two 3x3 rooms (MG-3 Fig. B.1(b)) and three 2x2 rooms (MG-4 Fig. B.1(c)). The goal of the agent, in MG-1, is to move and pick up the yellow ball and, in MG-2, MG-3 and MG-4, is to pick up a blue box which is located in the rightmost room, behind a locked door [4]. In these environments, the agent has six actions: turn left (L), right (R), move forward (F), pick up (PU), drop (D) and use (T) the object. With each new random seed, a new map is generated, including the agent’s initial position and the position of the objects. For MG-2, MG-3, and MG-4, there will always be an object obstructing the door. Specifically, for MG-3 and MG-4, the agent has to pick up a key with a matching colour to the door. In MG-3, we also introduce two distracted objects (the red ball and the green key in Fig. B.1(b)). All 3 environments are POMDP, meaning that the agent can only observe part of the map; the observation is an image tensor of shape [7,7,3]. The agent is equipped with six actions. Successfully reaching the goal within a predefined maximum number of steps results in a +1 reward for the agent; otherwise, it receives a 0 reward. The selected maximum number of steps for MG-1 is 270, MG-2 is 500, MG-3 is 1000 and for MG-4 is 5000. To complete these environments, the agent has to learn to move the ball by picking it up and dropping it in another location, then, it has to pick up the key, open the door and pick up the object in the other room.

B.2 Baseline Implementations

The backbone algorithm is Proximal Policy Optimization (PPO). We use the Pytorch implementation of this algorithm on the open-library Stable Baselines 3³. To enhance the performance of this backbone algorithm, we fine-tuned the entropy coefficient and settled on a value of 0.001 after experimenting with [0.001, 0.005, 0.01, 0.05]. All other parameters were maintained as per the original repository. Subsequently, we incorporated various intrinsic reward baselines on top of the PPO backbone, including Count-Based, Random Network Distillation (RND), ATTEN-

³<https://github.com/DLR-RM/stable-baselines3>

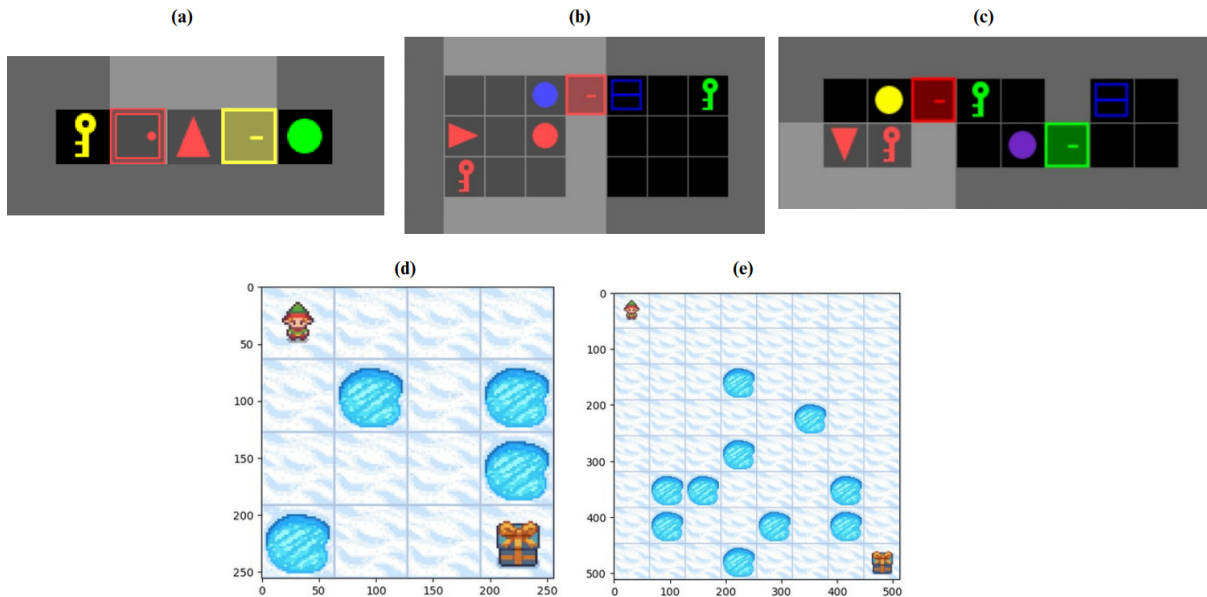


Figure B.1: (a): MG-1. (b): MG-3. (c): MG-4. (d): 4x4FL. (e): 8x8FL.

TION, CAI, and our VACERL.

For the Count-Based method, similar to the work of Bellemare et al. [2], we tracked the frequency of observations and associated actions and used the Simhash function to merge similar pairs [26]. The intrinsic reward is formulated as $r^+(o, a) = \frac{\alpha}{\sqrt{n(\phi(o, a))}}$, where $n(\phi(o, a))$ represents the count and $\phi(o, a)$ is the simhash function. We tune the exploration bonus hyperparameter α , however, there are no significant performance gains, as long as the bonus rewards do not overtake the rewards of the environment. Finally, we settle for a value of 0.001. We also test different values of the hashing parameters k of the Simhash function. The final implementation used $k = 256$, which shows the best results and is consistent with the referenced paper [2].

We also adopt a public code repository for the implementation of RND (MIT License)⁴. To align the implementation with our specific environments, we have made adjustments to the input shapes and modified the PPO hyperparameters to match those of other baselines. We adhered to the implementation provided in the code, using the hyperparameter values as specified.

In the case of ATTENTION, we leveraged the attention scores a_s from the encoder layer of the Transformer model as the reward signal. This approach has been used in the work of Pitis et al., [18] as a method to measure causal influence. The intrinsic reward has the form $r_{bonus}(o, a) = \alpha a_s(o, a)$. We integrate this as an iterative process similar to our VACERL framework and also aid the exploration in the earlier phase using Eq. 6 for fairness. Similar to our framework VACERL and the implementation of Count-based, we use an α value of 0.001 for this baseline.

Finally, for the CAI method, we measure the causal influence between each observation-action pair with the observation-action pair of the goal-reaching step [22]. This is slightly different from the implementation of the original paper, which assumes the knowledge of the location of the goal and other objects. Our final implementation used a two-layer MLP neural network to measure

⁴<https://github.com/jcwleo/random-network-distillation-pytorch>

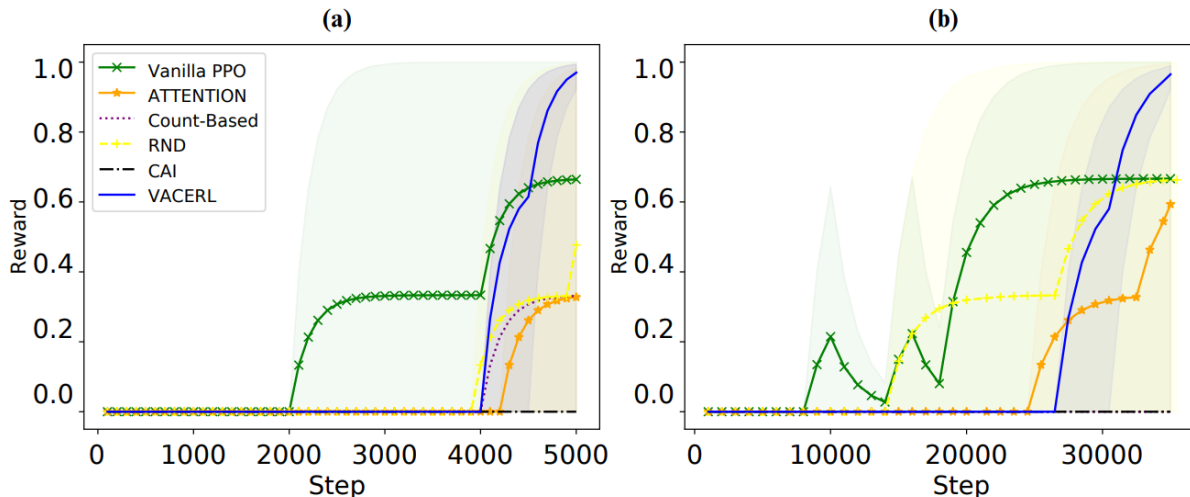


Figure B.2: Average return over 50 episodes (mean \pm std over 3 runs). Learning curve on (a) 4x4FL and (b) 8x8FL.

CAI and it is based on the code of the original paper (MIT License)⁵).

Additional details of hyperparameters can be found in Sec. D.

B.3 Additional Experiment Results

This section presents additional experiment results and visualization.

Learning Curve

The learning curves for the 4x4FL and 8x8FL tasks are illustrated in Fig. B.2; the learning curves for the MH-1 to MH-4 are illustrated in Fig. B.3, while the corresponding curves for MG-1, MG-3 and MG-4 are presented in Fig. B.5. The learning curves of VACERL in these figures show a similar pattern to the learning curves for MG-2 as presented in Fig. 2. Initially, the learning progress is slightly slower, as a number of training steps are required to acquire a correct causal representation. Subsequently, the performance accelerates rapidly, eventually surpassing baselines and attaining the optimal point.

The steps shown in these figures are the number of times the agent interacts with the environment, so for fairness, the number of steps of VACERL and causal baselines (CAI and ATTENTION) are computed as $H_s + a.T_s$, where a is the number of outer-loop iterations in line 7 of Algo. 1.

4x4FL Heatmap

The attention heatmap for the 4x4FL task is provided in Fig. B.6. These two figures show a similar pattern as in Fig. 4(a,b). Specifically, when the size of buffer B is small (Fig. B.6(a)), the accuracy of crucial step detection is not as precise compared to scenarios where the size of buffer B is larger (Fig. B.6(b)).

MG-2 Generated Causal Graph

The causal graph generated, as a result of our framework, for the MG-2 task is provided in Fig. 5. Each observation-action is associated with an image representing the map at the

⁵<https://github.com/martius-lab/cid-in-rl>

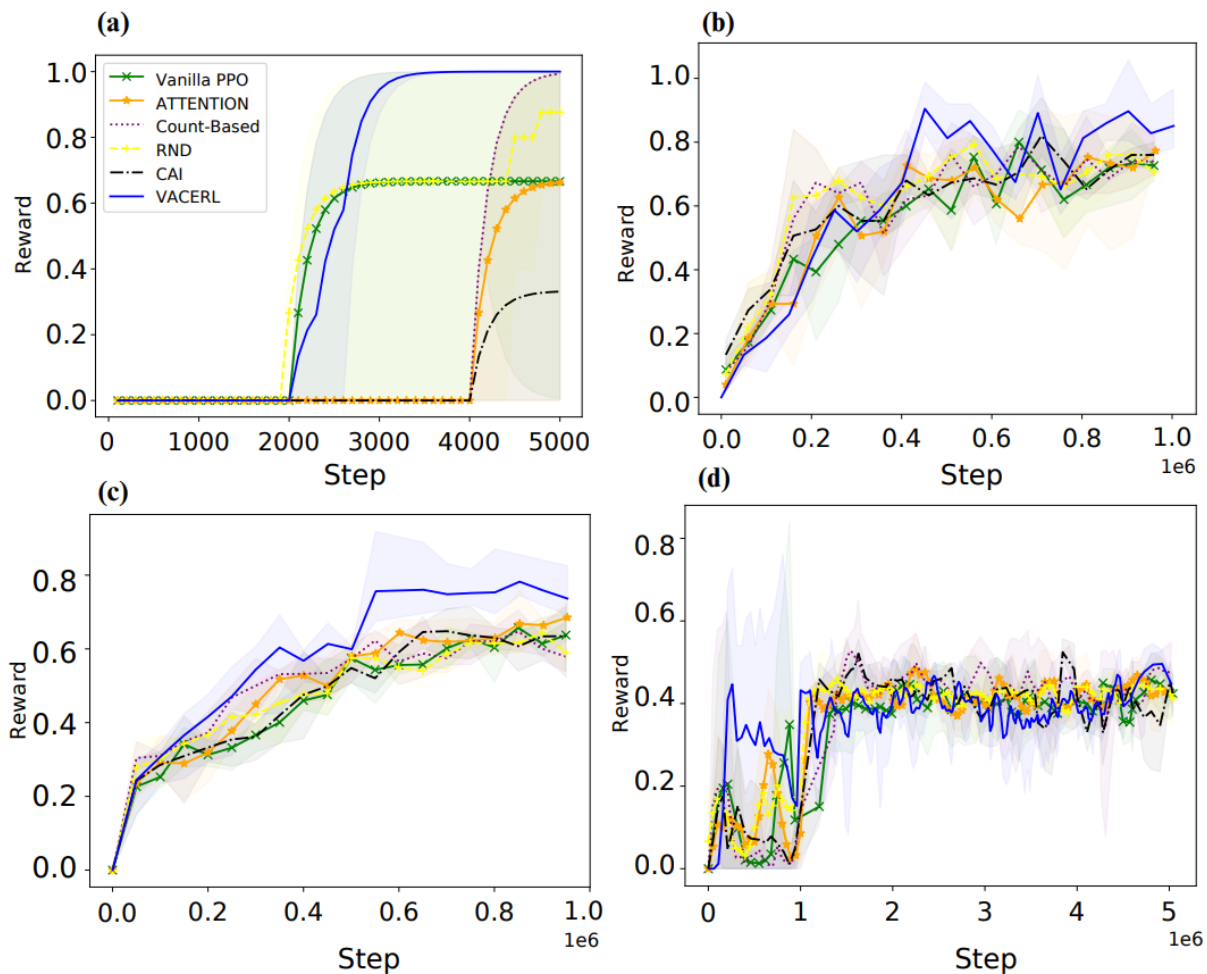


Figure B.3: Average return over 50 episodes (mean \pm std over 3 runs). Learning curve on (a) MH-1, (b) MH-2, (c) MH-3 and (d) MH-4.

timestep that the agent executes the action. Below is a summary of the relationships and our rationale for why the agent generated the unexpected, though reasonable, relationship. Expected relationships:

- Drop Key to Pick Up Goal.
- Open Door to Pick Up Goal.
- Pick Up Key to Drop Key.
- Pick Up Key to Open Door.
- Pick Up Ball to Drop Ball.

Unexpected Relationships:

- Drop Ball to Pick Up Goal and not to Open Door: We believe that this unexpected relationship is because the agent is allowed to repeat action that it has taken before in

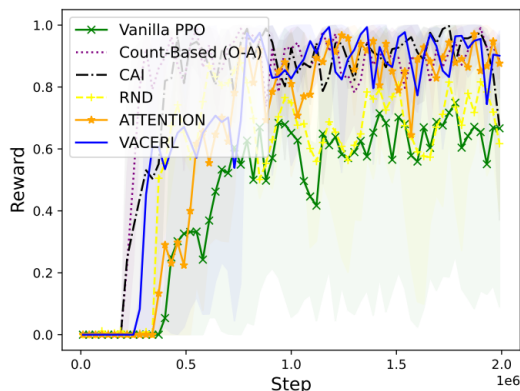


Figure B.4: Average return over 50 episodes (mean \pm std over 3 runs). Learning curve on MG-2 with vector input.

the environment. Consequently, the agent can pick up the ball again after it opens the door, thus affect the relationship between Drop Ball and Open Door. In addition, as the agent can only hold one item at a time, it must drop the ball before picking up the goal, which creates a relationship between Drop Ball and Pick Up Goal. If this sequence of steps frequently occurs in collected trajectories, the agent will infer that this sequence represents an accurate relationship, thus leading to the generation of this causal graph. Although this relationship is not what we expected, the relationship is not inaccurate, particularly in this environment wherein the agent can only hold a single item at a time.

C Setting to Test VACERL with Causal Subgoal for HRL

C.1 Environments

Both of the environments used in this section are available in Gymnasium-Robotics [11] and are built on top of the MuJoCo simulator [33]. The robot in question has 7 degrees of freedom (DoF) and a two-fingered parallel gripper. In FetchReach, the state space is $S \subset R^{10}$, and in FetchPickAndPlace, the state space is $S \subset R^{25}$. In both environments, the action space is $A \subseteq [-1, 1]^4$, including actions to move the gripper and opening/closing of the gripper. In FetchReach, the task is to move the gripper to a specific position within the robot’s workspace, which is relatively simpler compared to FetchPickAndPlace. In the latter, the robot must grasp an object and relocate it.

In both cases, user are given two values which are “achieved_goal” and “desired_goal”. Here, “achieved_goal” denotes the final position of the object, and “desired_goal” is the target to be reached. In FetchReach, these goals represent the gripper’s position since the aim is to relocate it. While in FetchPickAndPlace, they signify the block’s position that the robot needs to manipulate. Success is achieved when the Euclidean distance between “achieved_goal” and “desired_goal” is less than $0.05m$.

Sparse rewards are employed in our experiments, wherein the agent receives a reward of -1 if the goal is not reached and 0 if it is. The maximum number of timesteps allowed in these

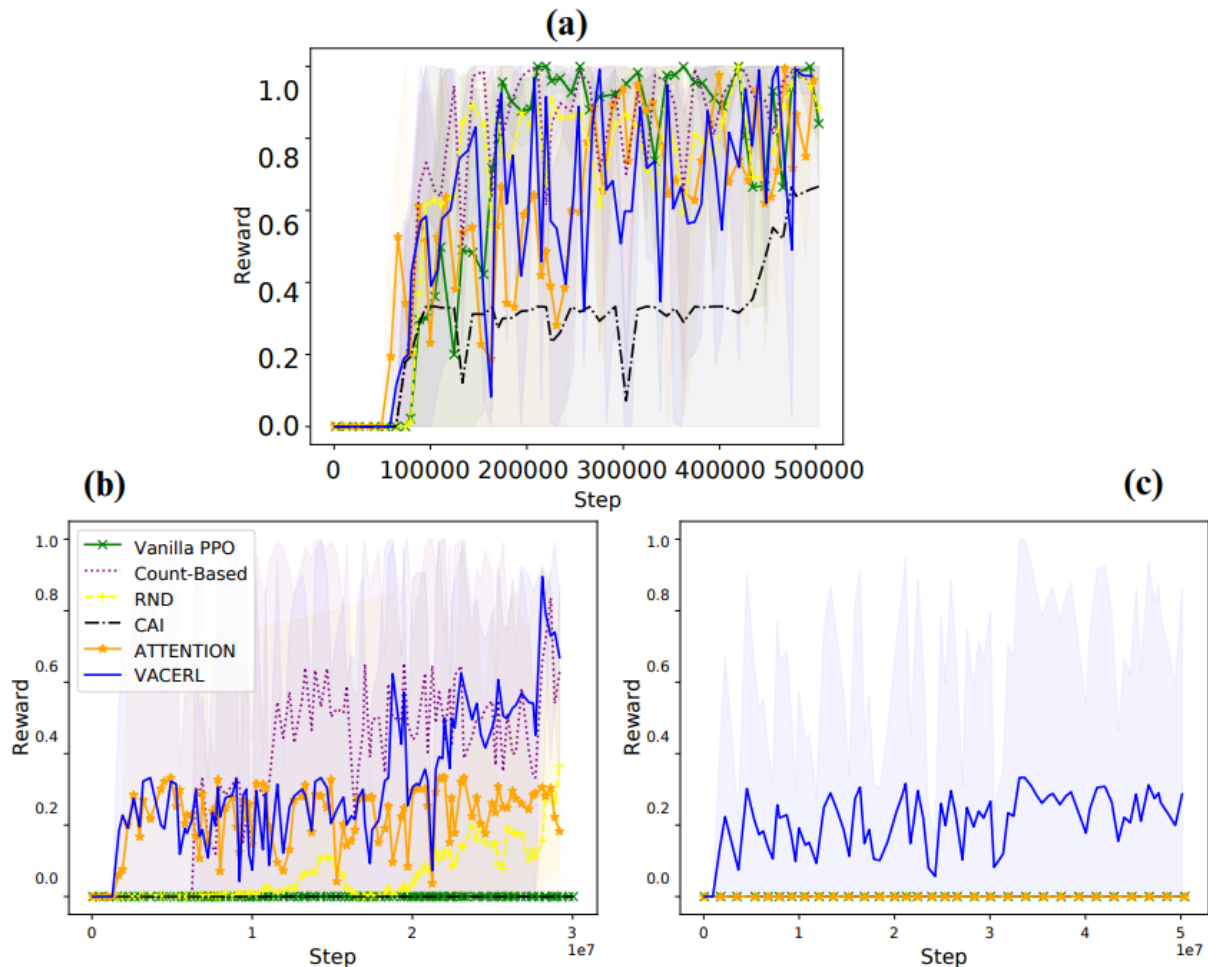


Figure B.5: Average return over 50 episodes (mean \pm std over 3 runs). Learning curve on (a) MG-1, (b) MG-3 and (c) MG-4.

environments is set to 100.

C.2 Baseline Implementations

We utilize the PyTorch implementation of DDPG+HER from the Stable Baselines 3 ⁶ open-library as one of our baselines. The hyperparameters for this algorithm are set to benchmark values available in RL-Zoo ⁷. We assess the performance of this baseline against the results presented in the original robotic paper by Plappert et al. [19], noting similarities despite differences in environment versions.

For our HAC implementation, the core algorithm of our approach, we adopt a publicly available code repository ⁸ (MIT License) by the author of the original paper [13]. We modify this code to align with our environments, where the goal position and the goal condition are supplied

⁶<https://github.com/DLR-RM/stable-baselines3>

⁷<https://github.com/DLR-RM/rl-baselines3-zoo>

⁸<https://github.com/andrew-j-levy/Hierarchical-Actor-Critic-HAC->

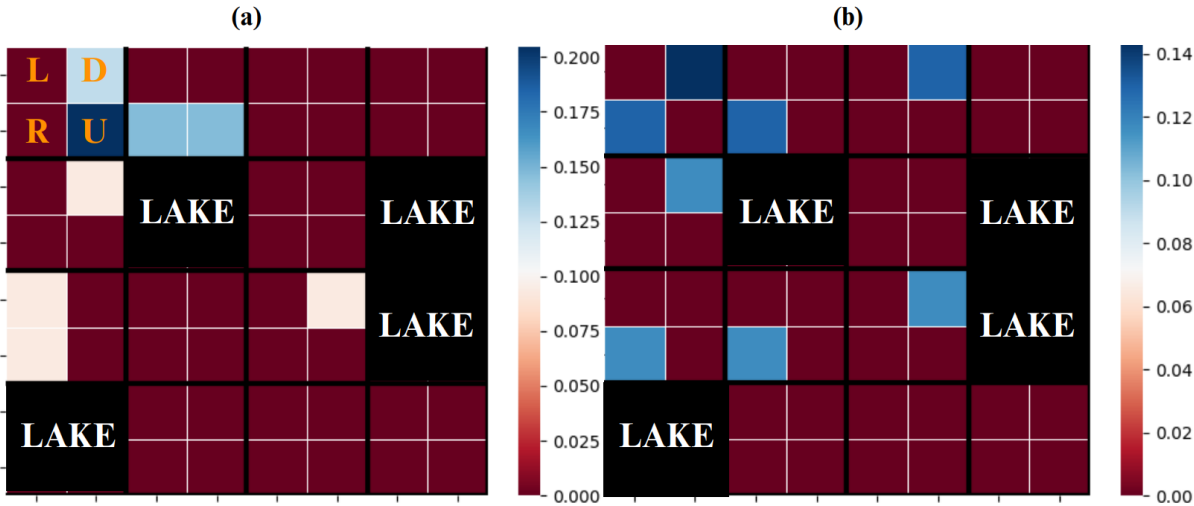


Figure B.6: (a,b): Attention heatmap when B has (a) 10 and (b) 100 trajectories for the 4x4FL task (Fig. B.1). We highlight the top-8 attended actions and their corresponding grids.

by the environments themselves. The baseline is implemented as a three-level DDPG+HER, in which the top two levels are used to supplied subgoals and the lowest level is used to learn the actions. We adjust the hyperparameters of the lowest level DDPG+HER to match those of the DDPG+HER baseline for fairness.

Additional details of hyperparameters can be found in Sec. D.

C.3 Additional Experiment Results

To validate our assertion that causal subgoals can effectively narrow down the search space for an HRL agent to significant subgoals, thus enhancing HRL sample efficiency in Robotic-Environments, we present an additional experiment along with the visualization of subgoals’ average coordinates selected by VACERL and Vanilla HAC in this experiment (Fig. C.1). The experiment was conducted in the FetchReach environment, with the causal graph re-evaluated every 2,000 steps, mirroring our main experiments. We specifically chose a run where initial subgoals of HAC and VACERL exhibited similar average coordinates (x, y, z) for fairness. In this run, the goal (indicated by a red + marker) was positioned at coordinates $(1.38294353, 0.68003652, 0.396999)$.

As illustrated in Fig. C.1(a), despite the initial subgoals’ average coordinates being very similar (represented by blue markers) $-(0.727372811, 0.501121846, 0.28868408)$ for HAC and $(0.7377534, 0.521795303, 0.2345436)$ for VACERL – VACERL swiftly converges to subgoals much closer to the goal after just one iteration of causal discovery learning, while, Vanilla HAC struggles to converge. We plot the weighted average coordinates of nodes in the causal graph after this iteration (indicated by a grey + marker), with weights determined by the probability of node sampling according to Eq. 7; higher probabilities correspond to higher weights. We choose to plot the values of this iteration because it represents the instance where VACERL undergoes the most significant shift in subgoals’ coordinates. The results indicate that the coordinates of nodes in the causal graph closely align with the coordinates of subgoals sampled by the top-level policy. This supports our intuition that causal subgoals contribute to the improvement in

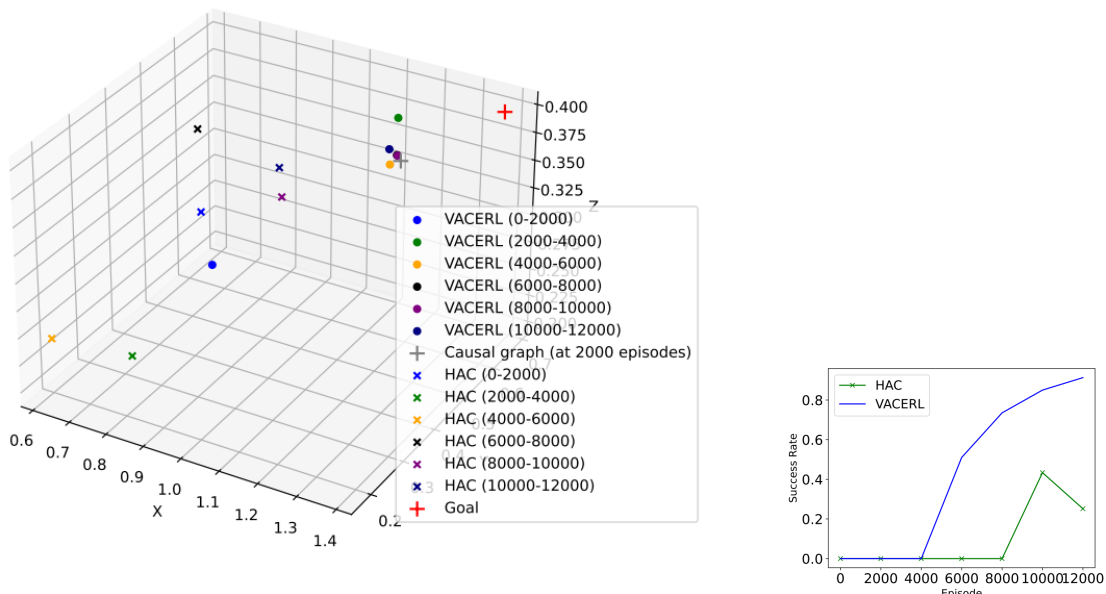


Figure C.1: **(a)**: The average coordinates (x, y, z) of subgoals selected by the top level policy in VACERL (both subgoals selected randomly and causal subgoals) and HAC at different training time intervals (the values in parentheses indicate the start and end episodes). The results are collected from a single run in FetchReach environment. **(b)**: The associated learning curve of the aforementioned run.

subgoal sampling and the overall sample efficiency of HRL.

The improvement is also reflected in the associated learning curve, in Fig. C.1(b), of the agent: after training for 4,000 episodes, VACERL begins to learn the environment, whereas HAC requires 8,000 episodes – coinciding with the point where the agent starts selecting subgoals with coordinates closer to the goal.

D Architecture and Hyperparameters of VACERL

The default hyperparameters (if not specified in accompanying tables then these values were used) are provided in Table. 2. The definitions and values for hyperparameters, which require tuning and may vary across different environments, are specified in the accompanying tables. The system’s architecture and the explanation for tuning of hyperparameter are outlined below:

Architecture

- *TF* model’s architecture: $num_encoder_layers = 2$, $num_decoder_layers = 2$, $hidden_size = 128$, $dropout = 0.1$.
- Functional model f_δ ’s architecture: 3-layer MLP, $hidden_size = 512$.
- PPO: Stable Baselines 3’s hyperparameters with entropy coefficient = 0.001.
- DDPG+HER: RL-Zoo’s architecture and hyperparameters for FetchReach and FetchPickAnd-Place environments.

- HAC: 3-levels DDPG+HER, architectures and hyperparameters are the same with DDPG+HER.

Tuning

- H_s (used for VACERL and all causal baselines): This hyperparameter requires tuning as it relies on the complexity of the environment. The more challenging the environment, the greater the number of head steps required to gather a successful trajectory and start the framework. For MG, FL, and MH environments, we use a random policy to collect this initial phase, however, in challenging robotic environments where collecting successful trajectories is difficult, we leverage the underlying HAC agent to gather these trajectories. Consequently, the value of H_s equals T_s in such environments. Additionally, H_s in MG, FL, and MH denotes the number of time the agent interacts with the environments, whereas in robotic environments, it denotes episode.
- M : This hyperparameter requires tuning as it depends on the state-space of the environment. Generally, a larger state-space requires a larger value for M . However, as shown in Fig. 4, too large M can introduce noise during the causal structure discovery phase and affect the final policy training result.
- ϕ_{sim} : This hyperparameter is only used in continuous space environments.
- T_s (used for VACERL and all causal baselines): Similar to H_s , this hyperparameter varies between environments. T_s in MG, FL, and MH denotes the number of steps the agent interacts with the environments, whereas in robotic environments, it denotes episode. T_s is also the number of steps/episodes before the causal graph is reconstructed.

Hyperparameters	Def.	Value
lr_{TF}	Learning rate of TF model	0.001
lr_{δ}	Learning rate of parameter δ	0.005
lr_{η}	Learning rate of parameter η	0.005
T	No. iteration causal discovery	10
F_s	Training steps for functional parameter	600
Q_s	Training steps for structural parameter	600
ϕ_{causal}	Causality threshold in Eq. 4	0.7
α	Intrinsic Coef.	0.001

Table 2: Default hyperparameters

Hyperparameters	Def.	4x4FL	8x8FL
H_s	Head steps to start the framework	2,000	15,000
M	Number of top attention steps	8	16
ϕ_{sim}	Similarity threshold in <code>is_sim</code> function.	-	-
T_s	Training steps of policy π_{θ}	2,000	8,000

Table 3: Hyperparameters that required tuning FL-Environments

Hyperparameters	Def.	MH-1	MH-2	MH-3	MH-4
H_s	Head steps to start the framework	500	10,000	10,000	10,000
M	Number of top attention steps	20	20	20	20
ϕ_{sim}	Similarity threshold in <code>is_sim</code> function.	0.9	0.9	0.9	0.9
ϕ_{causal}	Causality threshold in Eq. 4	0.6	0.6	0.6	0.6
T_s	Training steps of policy π_θ	2,000	200,000	200,000	500,000

Table 4: Hyperparameters that required tuning MH-Environments

Hyperparameters	Def.	MG-1	MG-2	MG-3	MG-4
H_s	Head steps to start the framework	2,000	300,000	800,000	1,000,000
M	Number of top attention steps	20	70	110	110
ϕ_{sim}	Similarity threshold in <code>is_sim</code> function.	0.9	0.9	0.9	0.9
T_s	Training steps of policy π_θ	50,000	300,000	1,000,000	10,000,000

Table 5: Hyperparameters that required tuning MG-Environments

Hyperparameters	Def.	FETCHPUSH	FETCHPICKANDPLACE
H_s	Head episodes to start the framework	20,000	100,000
M	Number of top attention steps	20	20
ϕ_{sim}	Similarity threshold in <code>is_sim</code> function.	0.9	0.9
ϕ_{causal}	Causality threshold in Eq. 4	0.6	0.6
T_s	Training steps of policy π_θ	20,000	100,000

Table 6: Hyperparameters that required tuning Robotic-Environments

Algorithm 1 VACERL framework.

Require: Environment env , policy π_θ , Buffer B , Transformer model TF , number crucial steps M , crucial step set $SCOAS$, and Dictionary D

- 1: Initialize $\pi_\theta, B, TF, SCOAS, D$
- 2: **for** $k = 1, 2, \dots, H_s$ **do**
- 3: Execute policy π_θ to collect $\{o_t^k, a_t^k\}_{t=1}^{T^k}$
- 4: **if** $reach_goal()$ **then** $B \leftarrow \{o_t^k, a_t^k\}_{t=1}^{T^k}$
- 5: **end if**
- 6: **end for**
- 7: **for** $iteration = 1, 2, \dots$ **do**
- 8: $D = \text{train_transformer}(TF, B, D)$ (Algo. 2) ▷ **Phase 1**
- 9: Define is_sim
- 10: Define $\mathcal{I}, SCOAS : i = \mathcal{I}((o_t^k, a_t^k)) \iff is_sim((o_t^k, a_t^k), (o, a)_i) = 1$
- 11: Sort D based on descending order of $D.values$
- 12: **for** key in $D.keys$ **do**:
- 13: **if** $SCOAS.length < M$ **then**
- 14: **if** $\mathcal{I}(key) \notin SCOAS$ **then**
- 15: $SCOAS \leftarrow key$
- 16: **end if**
- 17: **else**
- 18: **break**
- 19: **end if**
- 20: **end for**
- 21: Collect B^* using Eq. 1 ▷ **End Phase 1**
- 22: $G = \text{train_SCM}(B^*, SCOAS, \mathcal{I}, M)$ (Algo. 3) ▷ **Phase 2**
- 23: Extract causal tree from graph G ▷ **Phase 3**
- 24: **for** $k = 1, 2, \dots, T_s$ **do**
- 25: Train policy π_θ with r_{causal}^+ computed using Eq. 6 or with subgoal probability $P(i)$ using Eq. 7, and collect $\{o_t^k, a_t^k\}_{t=1}^{T^k}$
- 26: **if** $reach_goal()$ **then** $B \leftarrow \{o_t^k, a_t^k\}_{t=1}^{T^k}$
- 27: **end if**
- 28: **end for** ▷ **End Phase 3**
- 29: **end for**

Algorithm 2 Train Transformer.

Require: Transformer model TF , Buffer B and Dictionary D

```

1: for  $iteration = 1, 2, \dots, I$  do
2:   for  $k$  episodes in  $B$  do
3:      $(\hat{o}_T^k, \hat{a}_T^k) = TF(\{o_t^k, a_t^k\}_{t=1}^{T^k-1})$ 
4:     Compute  $\mathcal{L}_{TF}^k = MSE((o_T^k, a_T^k), (\hat{o}_T^k, \hat{a}_T^k))$ 
5:     if  $i==I$  then  $\triangleright D$  is only updated in the last training iteration
6:       if  $(o_t^k, a_t^k) \notin D.keys$  then
7:          $D[(o_t^k, a_t^k)] \leftarrow a_s$ 
8:       else
9:          $D[(o_t^k, a_t^k)] \leftarrow \max(a_s, D[(o_t^k, a_t^k)])$ 
10:      end if
11:    end if
12:    Update  $TF$  by minimizing loss  $\mathcal{L}_{TF}^k$ 
13:  end for
14: end for
15: return  $D$ 

```

Algorithm 3 Train Structural Causal Model.

Require: buffer B^* , crucial step set $SCOAS$, mapping function \mathcal{I} , Adam optimizer, M , functional parameter δ , structural parameter η , and adjacency matrix e

- 1: Initialize $\delta, \eta \in R^{M \times M}, e \in R^{M \times M}$
- 2: **while** T times iteration **do**
- 3: **for** $iteration = 1, 2, \dots, F_s$ **do**
- 4: $G \sim Ber((\sigma(\eta)))$
- 5: **for** $episode_k$ in B^* **do**
- 6: **for** step $t = 2, \dots, episode_k.length$ **do** \triangleright Start from the 2nd step of the episode
- 7: $Input = \{o_{t'}^k, a_{t'}^k\}_{t'=1}^{t-1} \wedge (\mathcal{I}(o_t^k, a_t^k)) \in PA(\mathcal{I}(o_t^k, a_t^k)) | G$
- 8: $Target = (o_t^k, a_t^k)$
- 9: $(\hat{o}_t^k, \hat{a}_t^k) = f_{\delta, \mathcal{I}(Target)}(Input)$
- 10: Compute $\mathcal{L}_{\delta, G}^k = MSE(Target, (\hat{o}_t^k, \hat{a}_t^k))$
- 11: $\delta \leftarrow Adam(\delta, \nabla_{\delta} L_{\delta, G})$
- 12: **end for**
- 13: **end for**
- 14: **end for**
- 15: **for** $iteration = 1, 2, \dots, Q_s$ **do**
- 16: **for** $episode_k$ in B^* **do**
- 17: **for** step $t = 2, \dots, episode_k.length$ **do**
- 18: $G^{(h)} \sim Ber((\sigma(\eta)))$
- 19: $Input = \{o_{t'}^k, a_{t'}^k\}_{t'=1}^{t-1} \wedge (\mathcal{I}(o_t^k, a_t^k)) \in PA(\mathcal{I}(o_t^k, a_t^k)) | G^{(h)}$
- 20: $Target = (o_t^k, a_t^k)$
- 21: $(\hat{o}_t^k, \hat{a}_t^k) = f_{\delta, \mathcal{I}(Target)}(Input)$
- 22: Compute $\mathcal{L}_{\delta, G^{(h)}}^k = MSE(Target, (\hat{o}_t^k, \hat{a}_t^k))$
- 23: $i = SCOAS.index(\mathcal{I}(Target))$
- 24: **for** $item$ in $SCOAS$ **do**
- 25: **if** $item$ in $Input$ **then**
- 26: $j = SCOAS.index(\mathcal{I}(item))$
- 27: $\eta_{ij} \leftarrow \eta_{ij} - \beta(\sigma(\eta_{ij}) - e_{ij}^{(h)}) \mathcal{L}_{\delta, G^{(h)}}^k$
- 28: **end if**
- 29: **end for**
- 30: **end for**
- 31: **end for**
- 32: **end for**
- 33: **end while**
- 34: **for** $i = 1, 2, \dots, M$ **do**
- 35: **for** $j = 1, 2, \dots, M$ **do**
- 36: **if** $\eta_{ij} > \eta_{ji}$ and $\sigma(\eta_{ij}) > \phi_{causal}$ **then** $\triangleright \phi_{causal} = 0.7$
- 37: $e_{ij} \leftarrow 1$
- 38: **else**
- 39: $e_{ij} \leftarrow 0$
- 40: **end if**
- 41: **end for**
- 42: **end for**
- 43: $G = \{e_{ij}\}$
- 44: **return** G
